

Simulations of Laser Ablation of Poly(methyl methacrylate): Fluence versus Number of Photons

Patrick F. Conforti, Manish Prasad, and Barbara J. Garrison*

Department of Chemistry, 104 Chemistry Building, Penn State University, University Park, Pennsylvania 16802

Received: April 13, 2007; In Final Form: May 25, 2007

Using molecular dynamics simulations with an embedded chemical reaction scheme, two pathways of chemical decomposition of poly(methyl methacrylate) leading to ablation are independently investigated using two photon energies. The model employed in this study uses a coarse-grained substrate with predetermined reaction channels and a fixed penetration depth. The simulations allow for single-photon absorption per site with the possibility of photochemical bond cleavage. Within these parameters, the absorption of 7.9 and 5 eV photons (equivalent to 157 and 248 nm radiation, respectively) is simulated over a range of fluences to demonstrate the fundamental photochemical effects of the number of photons versus the total energy absorbed. Above the ablation threshold, similar mechanisms of ejection occur using either photon energy, but, at equal fluences, more material is ejected with a larger number of lower energy photons. When more photons are absorbed cleaving a greater number of bonds, more transformation occurs deeper within the substrate, and the amount of ejected material increases. If thermal as well as photochemical processes occur, the ablation threshold is shifted to a higher fluence. The amount of residual photon energy following the bond scission affects the ablation plume composition.

Introduction

Laser ablation is playing an increasingly important role in application development as tools and methods shift further into the nanoscale. The introduction of ultraviolet (UV) laser ablation has been effective in advancing many applications such as drilling ink-jet nozzles¹ and developing lab-on-chip devices.² Many experiments have been performed and many models have been developed in order to gain an understanding of the material–light interaction and the processes that drive ablation in polymeric materials with the expectation to further optimize current technology.^{3–10} A full microscopic insight, however, has eluded these investigations due to the complex interplay between the laser and the material. Molecular dynamics (MD) simulation is ideal for this fundamental task as it can resolve the irradiation process into microscopic details and shed light on the mechanisms that contribute to material ejection.^{11–15}

Many experimental investigations have probed the mechanisms of ablation for the material poly(methyl methacrylate) (PMMA). These studies have varied over the parameters of laser wavelength, pulse width, and fluence. Initial studies of PMMA ablation by Srinivasan et al. used wavelengths of 193 and 248 nm with fluences above the threshold and analyzed the ejected material—a majority of which was comprised of smaller oligomers of PMMA.^{16,17} In addition, the yield consisted of lesser amounts of C₂, CO₂, and MMA monomer with more monomers for the 193 nm experiments. Srinivasan concludes that the main mechanism for both wavelengths involves the photochemical decomposition of material preceding the ejection of small molecules and gases that aid in the transport of the large pieces of material. Using a range of nanosecond pulse widths, Srinivasan also observes an optimal pulse width and delay time between pulses to maximize the etch depth.¹⁸ Stuke

and co-workers describe material ejection using the interaction of 193 and 248 nm radiation with 2,2,4,4-tetramethylglutaric acid, dimethyl ester which is used as a model compound of PMMA.¹⁹ The results, which do not differ significantly with changing wavelength, show that the side chain is preferentially broken releasing such products as CO₂, methane, CO, methanol, and methyl formate with only a minor amount of MMA formed. The remaining compound incubates producing double-bonded carbon sites in the chain. Srinivasan also observed incubation in PMMA using 193 and 248 nm radiation.²⁰ Unsaturated PMMA polymers formed through incubation were experimentally determined by Krajnovich to more strongly absorb the UV photons which led to the thermal ejection of lower molecular weight fragments with masses less than 150 amu.²¹ Following the incubation described by both Stuke and Krajnovich, further studies at 248 nm show that cleavage of the main chain bond and thermally activated unzipping of the MMA monomer ensues.²² Ablation studies of PMMA at 157 nm indicate a high photochemical component of material breakdown similar to that of the longer 193 and 248 nm wavelengths with mass loss attributed to side chain cleavage.^{23,24} At wavelengths above 248 nm, thermal mechanisms rather than photolytic bond breaks dominate the breakdown of PMMA and lead to the ejection of large amounts of monomer and monomer fragments.^{25,26} The collective picture of the process using the sum of these investigations remains unclear but shows the degree of variation in the description of the ablated material and the potential mechanisms of ablation.

MD simulations have shown to be particularly useful in giving insight into how the microscopic processes involved with laser irradiation result in ablation for PMMA.^{27–30} For these studies, a hybrid Monte Carlo-MD simulation protocol was developed in which photons directly cleave bonds, and activated chemical reactions ensue.³¹ A comprehensive analysis of the photothermal and photochemical interaction of 7.9 eV photons (157 nm

* Corresponding author. E-mail: bjj@psu.edu.

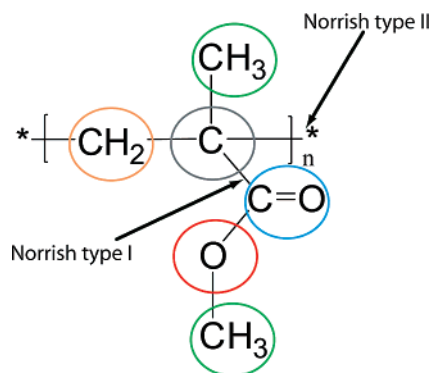


Figure 1. Structure of a PMMA molecule. The circles group the coarse-grained beads used in the simulations. The Norrish type I and Norrish type II breaks used in the simulations are also denoted.

radiation) with a PMMA substrate was performed.²⁷ The ablation studies were conducted over a range of fluences for 5 and 150 ps pulse widths. In addition, three different channels of photon absorption were simulated *separately* in order to assess the effects each has on the ejection mechanism and plume composition. In one channel, the photothermal case, absorption was simulated by heating monomers in the polymer sample. In the two other channels, photochemical absorption of a photon either led to the cleavage of the main chain bond or the side chain bond in the polymer. Following the photochemical scissions, further chemical reactions occurred in the simulations according a Monte Carlo scheme.

For each of the photothermal and photochemical simulations, ablation was observed to occur above a threshold fluence. With the longer 150 ps pulse width, pure photothermal simulations elucidated a mechanism in which the energy deposited in the sample induced a critical number of bonds to thermomechanically break and material to eject. In the photochemical cases with the 150 ps pulse, the connectivity of the polymer chain was disrupted following a photolytic scission, the cohesive energy decreased, and the amorphous substrate chemically transformed and fragmented. In one pathway of chemical breakdown (Norrish type I, see Figure 1), small molecules and gases were formed and released which hollowed out the substrate. Thermal induced ejection of large clusters of polymer having low velocities followed. In another pathway of chemical decomposition (Norrish type II, see Figure 1), the polymer chain unzipped to form monomers. The monomer formation disrupted the connectivity of the polymer, and the thermally driven ejection of clusters occurred in a layer-wise manner. Both photochemical ablation processes occurred in two steps: the photolytic scission of bonds leading to subsequent reactions fragmenting the substrate followed by the thermally driven ejection of large fragments of material. For the shorter 5 ps pulse width simulations, there was high compressive pressure present which was absent using the 150 ps pulse. The amount of molecules ejected from the substrate, however, did not significantly differ at any given fluence between the two pulse widths. For the 5 ps photothermal simulations, the fast deposition of heat created pressure gradients in the material. The high-pressure provided higher liftoff velocities but did not influence the ejection process which was established to be thermal in nature. For the 5 ps photochemical simulations, decomposition of the system occurred analogous to the longer pulse widths, but the formation of the reaction products occurred more rapidly. Similar to the photothermal simulations, the pressure and heat that developed as a result provided higher ejection velocities but did not significantly change the mechanism of ablation.

TABLE 1: Number of 7.9 and 5 eV Photons Absorbed at Fluences Ranging from 4 to 15 mJ/cm² for a 51 × 51 Å² Substrate Area

fluence/mJ cm ⁻²	number of photons	
	7.9 eV	5 eV
4	825	1303
5	1031	1629
6	1237	1955
7	1443	2280
8	1650	2606
9	1856	2932
10	2062	3258
12	2475	3910
14	2887	4561
15	3094	4887

In this study we extend the discussion regarding the photochemical effects of the material-light interaction in PMMA to a comparison between two photon energies. Experimental investigations into the basic mechanisms of laser ablation have underlying obstacles which accompany a change in wavelength including variation in the penetration depths and branching ratios as well as the difference in photon energy.¹⁹ The advantage of using molecular simulation is that such variations can be studied in a systematic approach in order to assess each of their effects. Here, MD simulations are analyzed along a range of fluences for two photon energies which are of experimental interest, 7.9 eV/photon and 5 eV/photon equivalent to 157 and 248 nm radiation, respectively, while keeping the other parameters constant (including penetration depth, decomposition pathways, and possible chemical reactions). While these conditions do not allow the simulations to map directly to experiment and interpret the results, the fundamental physics associated with the differences in photochemistry and energy can be analyzed. In the simulations, the influence of the number of photons versus the total energy deposited is investigated, and their effects on the ablation yield as well as substrate and plume characteristics are compared and contrasted. The simulations highlight the essential physical and chemical differences that occur using two different energy photons and help unravel some of the experimental complexity that accompanies the ablation phenomenon.

Computational Details

MD simulations are used to study the photochemical interaction of light with PMMA. Photons of 7.9 and 5 eV (equivalent to 157 and 248 nm radiation, respectively) are absorbed by the substrate for fluences of 4–15 mJ/cm². The number of photons absorbed by the sample at each fluence is given in Table 1. The photon energies are chosen to be greater than 4.7 eV/photon with the intention that the corresponding wavelengths are less than 266 nm radiation, a region where the photochemical processes dominate.²⁵ The absorption site of each photon is chosen randomly with the probability attenuated by Beer's Law using a penetration depth of 100 Å for both photon energies. Even though the absorption characteristics of PMMA differ according to the wavelength with weak absorption at 248 nm and strong absorption at 157 nm³², the simulations do not include this distinction. Following photon absorption, either the main chain C–CH₂ bond (Norrish type II) or the side chain C–CO bond (Norrish type I) is directly cleaved to form their respective radicals (see Figure 1).³³ The strength of either bond is approximately 3.6 eV; the excess energy of each photon goes into heat. Each type of bond break (Norrish type I or II) is simulated separately in order to assess the effects of one set of reactions that might result following laser irradiation. Following

the formation of radicals, further reactions are possible which are discussed below. The reactions include the unzipping of the monomer from the polymer chain, which can absorb a photon (with the same probability as a main chain carbon) as heat rather than causing a bond scission. Monomer absorption is the only situation in the photochemical simulations where photons are absorbed as heat due to the C=C bond strength. The simulations will therefore have higher quantum yields than in experimental studies¹⁹ to maximize photochemistry in the system and observe its effects. Pulse widths of 5 and 150 ps are chosen to examine two different ablation regimes—with and without pressure buildup in the sample.²⁷ Using short pulses, multiphoton absorption could occur,³⁴ however, the simulations limit one photon absorption per carbon center. Each of these assumptions is made in the simulation so the effects of fluence and the accompanying number of photons on ablation can be examined independent of other parameters.

A scheme has been developed which allows further activated chemical reactions to occur during the MD simulation using an embedded Monte Carlo scheme following the formation of radicals by photons. The simulation protocol is based on the coarse-grained chemical reaction model developed by Yingling and Garrison,³⁵ and exact details of the method will be described elsewhere.³¹ Briefly, each radical site has a set of reaction pathways available with associated activation and reaction energies. During the dynamics calculation, a survival probability of a radical is calculated using its simulation existence time and rate constant. The rate constant is determined by summing all possible Arrhenius reaction rates of the reacting radical with each computed one using the local temperature, the activation energy of a particular reaction, and the Boltzmann constant. The radical is able to react when a randomly chosen number is greater than the survival probability. A reaction is then attempted by comparing another random number with the normalized reaction rates of each possible reaction pathway. The chosen reaction is then performed by changing the reactant species to products and measuring the change in potential energy. If the change is within 10% of the reaction energy, the reaction is accepted, the reactants are replaced with products, and the kinetic energy of the system is changed to correspond with the energy difference. If not, the reactants remain unchanged, and they continue in the MD simulation and attempt to react again at a later time step.

The reaction pathways included in the simulation are chosen as a representative set based on experimental results.^{17,19,36} Following the Norrish I type break, Figure 2a, the methyl formate radical is able to decompose into CO₂ and a methyl radical (1), decompose into CO and a methoxy radical (2), or abstract a hydrogen to become methyl formate (3). The resulting methyl radical and methoxy radical each can abstract hydrogen (4 and 5), and radical–radical recombination reactions can occur on the main polymer (6 and 7). Following the Norrish type II break, Figure 2b, the polymer radicals are able to unzip into monomer units (1 and 2), abstract hydrogen (3 and 4), or eliminate a methyl radical and terminate the polymer with a double bond (5). The resulting methyl radical can abstract hydrogen to become methane (6), and radical–radical recombination reactions can occur to form double bonds on the main chain (7 and 8). The activation and reaction energies for each of these reactions have been calculated or taken from the literature.^{37,38} These reactions used in the simulations are by no means the entire set of possibilities but contain the essential processes including formation of small molecules, monomers,

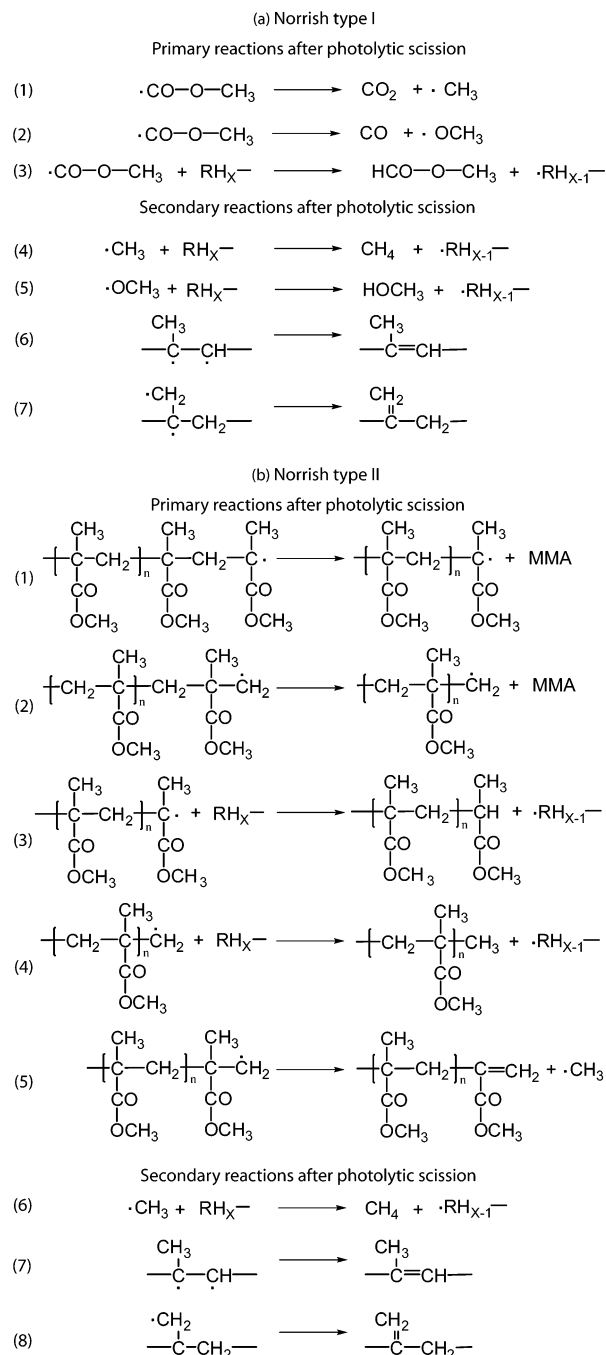


Figure 2. Radical chemistry following the photolytic scission used in the MD reaction scheme: (a) the Norrish type I primary and secondary reactions and (b) the Norrish type II primary and secondary reactions.

and double bonds which chemically change the composition of the substrate and affect the ablation process.

The simulation consists of coarse-grained PMMA substrate with a united atom representation of the functional groups C, CH₂, CH₃, C=O, and O of the polymer chain (Figure 1) as well as CH₄, OH, and CH groups which are formed as a result of chemical reactions. Coarse-grained beads are used in order to increase the time step of the simulation by eliminating the computationally expensive CH and C=O bond vibrations which are not essential in observing the mesoscopic motion of ablation.^{14,30} The potentials used in the simulation have been previously described and allow for bonds to mechanically break under conditions of high temperature and stress.^{30,39} The substrate consisting of 951 PMMA chains (19 monomer units per chain) is initially constructed in a computational cell using

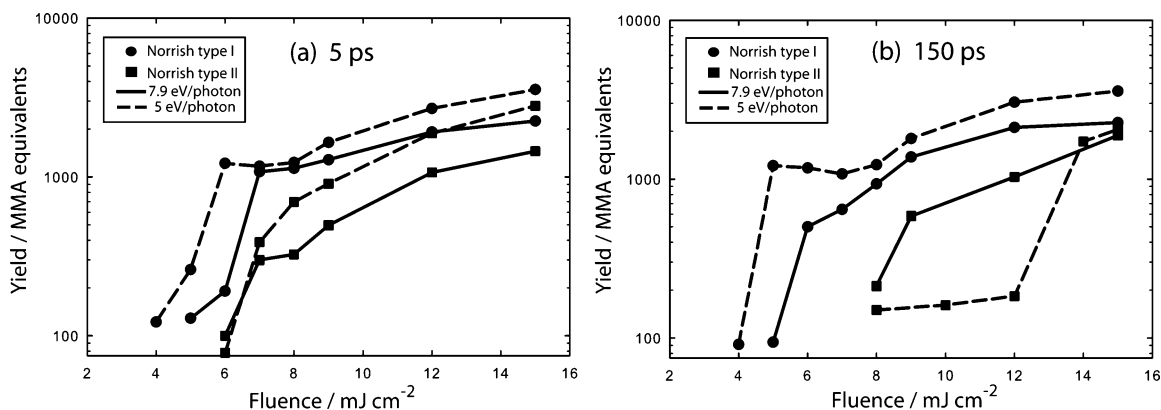


Figure 3. Yield in MMA equivalents plotted as a function of fluence for (a) a 5 ps pulse width and (b) a 150 ps pulse width. The Norrish type I results are circles (●), and the Norrish type II results are squares (■). The solid lines are the yield for 7.9 eV/photon simulations, and the dashed lines are the yield for 5 eV/photon simulations.

a self-avoiding walk at low density and then gradually compressed until a density of 1.19 g/cm^3 is attained corresponding to a $51 \times 51 \times 936 \text{ \AA}^3$ sample size. Periodic boundary conditions are imposed in the surface plane simulating the center of the laser. At the bottom of the sample, a pressure-absorbing boundary condition is used which mimics an infinitely long sample and prevents the reflection of a propagating pressure wave as a result of the excitation pulse.⁴⁰

Results and Discussion

1. Ablation Yield. The ablation regimes for 7.9 eV photons and 5 eV photons are established by plotting the yield of particles in MMA equivalents as a function of fluence for 5 and 150 ps pulse widths, parts a and b of Figure 3, respectively. The yield is calculated by dividing the sample based on density into a bulk substrate (density greater than 0.2 g/cm^3) and an ejected plume (density less than 0.2 g/cm^3). The density of 0.2 g/cm^3 is not critical to characteristics of either the substrate or the plume as the density decreases rapidly at the interface. When there is a discontinuous jump from tens of MMA equivalents to several hundred MMA equivalents ejected following laser excitation, the ablation regime is realized. The threshold fluence lies between 4 and 6 mJ/cm^2 for the Norrish type I case regardless of pulse width and wavelength, and for the Norrish type II case, the threshold fluence varies between 7 and 13 mJ/cm^2 depending on pulse width and wavelength used. The characteristic mechanism for ejection below the ablation threshold is mainly desorption of small molecules, such as CO_2 , CO , CH_4 , MMA monomers, and monomer fragments. Similar mechanisms have been described for subthreshold ejection of molecules in simulations of organic solids⁴¹ and chlorobenzene.¹³ An average cluster size of hundreds of MMA units is observed in the plume for each simulation that exhibits ablation. Clusters are determined by grouping together molecules regardless of their bonding characteristics within 5 \AA , as all the bonding potential energies go below the available thermal energy with a separation of $3\text{--}5 \text{ \AA}$. Average cluster size is determined by the ratio of the second moment of the cluster size distribution to its first moment. An analysis of the ablation plume shows that a majority of its makeup consists of sizable clusters between 240 and 1900 MMA units and also includes small gaseous particles, MMA monomers, and polymer fragments. The presence of large clusters in the plume is indicative of the ablation regime.⁴¹

The disparity in the ablation yield with varying photon energy at a given fluence is due to the effect of the different number of photons. The basic process that results in ablation following

the irradiation of the polymer substrate, though, is the same regardless of the photon energy. As explained in a previous study, the photochemical cleavage of a bond (either Norrish type I or II) disrupts the polymer connectivity, decreases the cohesive energy, and allows the substrate to transform, fragment, and eject.²⁷ For discussion here of the comparison between fluence versus number of photons, Figure 4 displays a contour plot of the fraction of original polymer converted to products by reactions in the top 500 \AA of the polymer substrate as a function of depth below the initial surface and time for (a) a 7.9 eV/photon, Norrish type I simulation, (b) a 5 eV/photon, Norrish type I simulation, (c) a 7.9 eV/photon, Norrish type II simulation, and (d) a 5 eV/photon, Norrish type II simulation, each with a fluence of 15 mJ/cm^2 and a pulse width of 5 ps. The contour color in each plot designates the fraction of the beads in a 10 \AA slice that have been transformed into the reaction products shown in Figure 2, such as CO , CO_2 , CH_4 , CH_3OH , HCOOCH_3 , MMA, and double-bonded carbon. For example, a value of 0 (blue) would indicate the original pristine material, while a value of 1 (red) would indicate that the material has been completely transformed into new products. The jagged jumps in the plots of the material occur as large pieces of the substrate eject and are then considered as yield, or ablated material. Activated reactions take place $1\text{--}2 \text{ ps}$ after the radicals are formed; therefore, by 15 ps most of the transformation has been completed for the 5 ps pulse width simulations. In the Norrish type I simulations, the dominant reactions include the formation of CO_2 , CH_4 , and double-bonded carbon. In the Norrish type II simulations, the dominant reactions include the formation of MMA and double-bonded carbon on the main chain. Due to the presence of more photons at a given fluence (Table 1), higher fractions of material transformation occur deeper in the material for the 5 eV/photon simulation compared with the 7.9 eV/photon simulation as shown in the plots of Figure 4. For example, with a fluence of 15 mJ/cm^2 , 680 eV of energy is deposited in a 25 \AA slab at a depth of 200 \AA beneath the substrate surface. For the 7.9 eV/photon simulation, this amount of energy corresponds to 86 photons compared with the 5 eV/photon simulation where the energy corresponds to 136 photons. The greater number of photons cleaves more bonds, creates more radicals and allows for a greater number of reactions to occur farther below the surface of the substrate. Since more material transformation occurs (more reactions transpiring), the swelling of the surface is $50\text{--}100 \text{ \AA}$ greater prior to ablation for the 5 eV photon simulations. Additionally, significant chemical damage penetrates 80 to 100 \AA farther into the substrate for the 5 eV photon simulations. In most cases, the eventual ejection

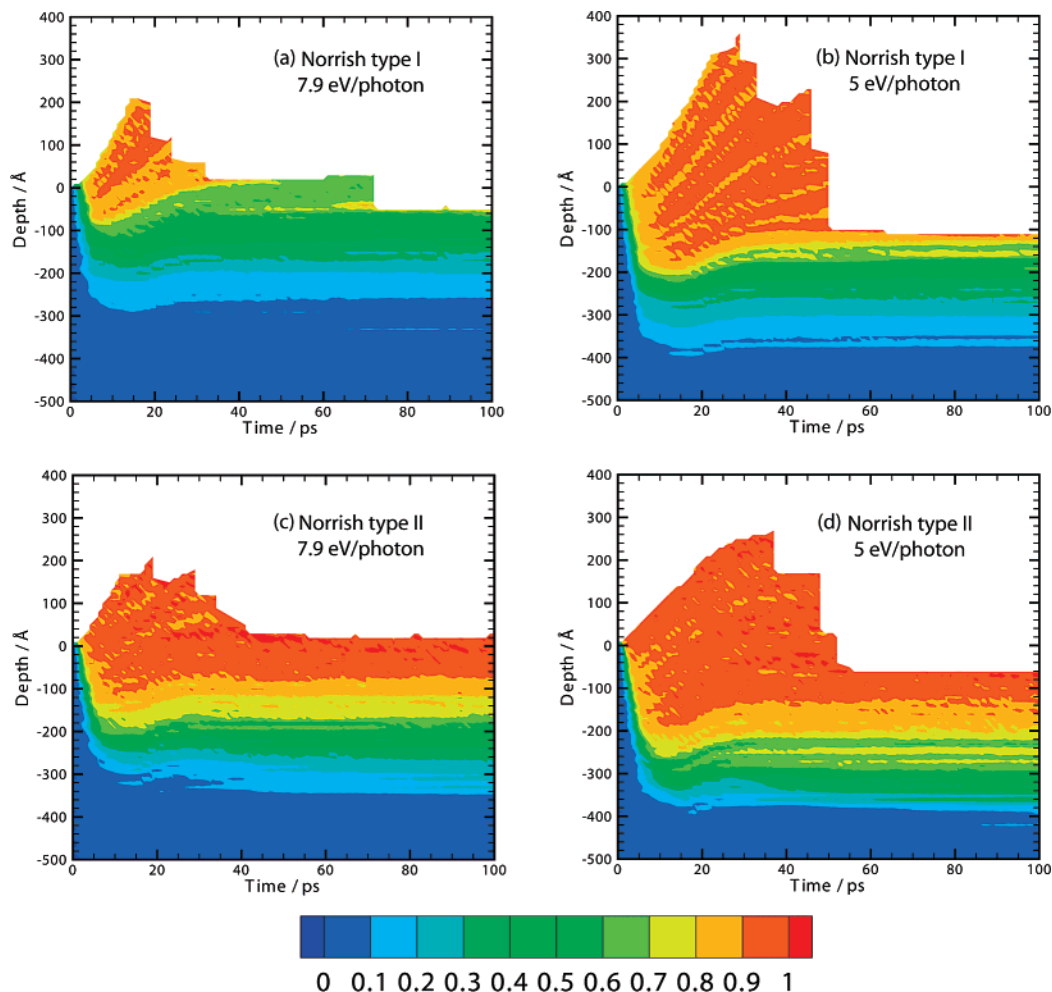


Figure 4. Contour plots of the fraction of original polymer converted to products by reactions in the substrate as a function of depth from the initial surface and time for (a) 7.9 eV/photon Norrish type I simulation, (b) 5 eV/photon Norrish type I simulation, (c) 7.9 eV/photon Norrish type II simulation, and (d) 5 eV/photon Norrish type II simulation for a 15 mJ/cm² fluence and a 5 ps pulse width.

of more material using 5 eV photons is a direct result of this greater transformation with more of the material fragmenting, weakening the integrity of the substrate, and allowing for liftoff of material from deeper within the substrate.

2. Mechanisms of Ablation. For the short pulse simulations, the ejection mechanism is dominated by the creation of small molecules, high temperatures, and high compressive pressure. As previously stated, chemical reactions occur within 1–2 ps after bond cleavage, many of which are exothermic in nature, particularly the double-bond formation which deposits a large amount of energy in the substrate. In addition, the residual photon energy following the bond cleavage increases the kinetic energy of the system. After each photon absorption and subsequent bond scission, approximately 4.3 or 1.4 eV of energy remains from a 7.9 or 5 eV photon, respectively. This excess energy is added to the kinetic energy of the participating radicals. As a result, prior to ablation, the maximum temperature in the top 100 Å of the substrate (one penetration depth) is higher for the 7.9 eV Norrish type I or II simulations than for the 5 eV Norrish type I or II simulations. For both wavelengths, this deposition of heat in the sample drives the thermal ejection of substrate. The rapid addition of heat and formation of many gases and monomers also creates a pressure gradient in the substrate in a process described as thermochemical pressure generation.⁴² Maximum pressures of 4.4 and 6.9 GPa are observed using a fluence of 15 mJ/cm² for 7.9 eV/photon and 5 eV/photon Norrish type II simulations, respectively. As

discussed, simulations have shown that the high pressure causes the rapid and violent (high velocity) ejection of the gases and some polymer clusters.²⁷

A similar ejection process occurs for the longer 150 ps simulations with 5 eV versus 7.9 eV photons as for the described 5 ps simulations. However, there is no propagating pressure wave present as a result of the laser pulse in contrast to the 5 ps pulse. For the 150 ps simulations, the reactions take place throughout the longer pulse duration, and the eventual ejection is not as explosive due the gradual formation and removal of small molecules.²⁷ The ejection mechanism still occurs analogous to that of the 5 ps simulations with the production of gases hollowing out the substrate and preceding the release of large clusters for the Norrish type I case. At equal fluences for the Norrish type I simulations with a 150 ps pulse width, more transformation of material occurs deeper in the substrate using a greater number of 5 eV photons, and more material is ablated. For the Norrish type II case, the formation of MMA disrupts the connectivity of the polymer before layers of substrate are removed. Due to the nature of photon absorption in the simulation, the ablation threshold for the set of Norrish type II simulations using a 150 ps pulse with 5 eV/photon, though, is shifted to a higher fluence, Figure 3b. This shift can be attributed to the length of the pulse width in relation to the time scale of the unzipping reaction and the thermal effects of the 5 eV photons which are discussed below. The generation of MMA follows directly from a Norrish type II bond scission and

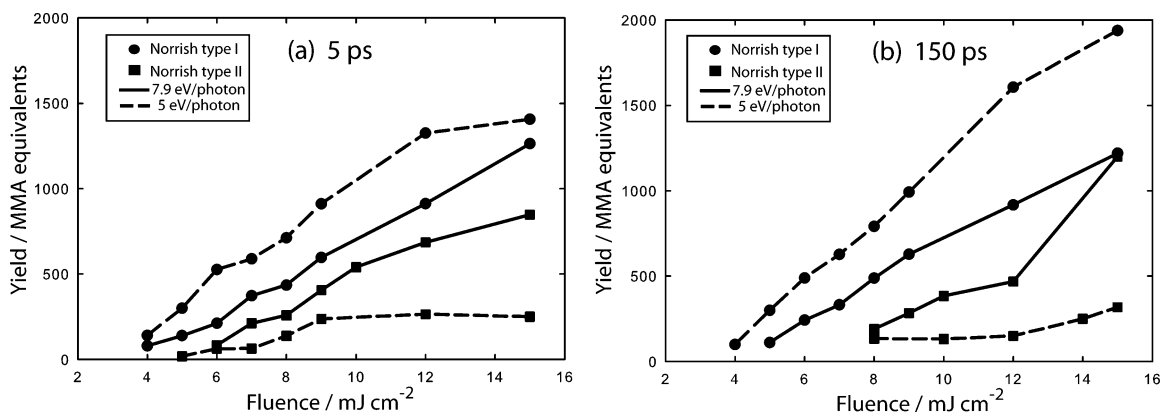


Figure 5. The yield of particles less than or equal to one MMA monomer in size plotted as a function of fluence for (a) a 5 ps pulse width and (b) a 150 ps pulse width. The Norrish type I results are circles (●), and the Norrish type II results are squares (■). The solid lines are the yield for 7.9 eV/photon simulations, and the dashed lines are the yield for 5 eV/photon simulations.

propagates along the polymer chain eventually producing more than 1 monomer per photon-induced bond break. In the simulation, a MMA monomer, however, can only absorb a subsequent photon as heat. When the pulse width is 150 ps, activated unzipping occurs during the pulse, and, as a consequence, a significant amount of photons are then absorbed as heat by MMA monomers in the simulation. It has been previously shown in simulations that the energy density in the substrate must be above a critical value to initiate pure thermal ablation.^{27,43} Using 7.9 eV photons, ablation is able to occur solely due to pure heating of the PMMA substrate with the number of photons absorbed at a fluence of 10 mJ/cm².^{27,43} However, the amount of 5 eV photons that are absorbed in the surface volume do not supply enough energy to cause mechanical failure and initiate pure thermal ablation at a comparable fluence.⁴³ Though the polymer becomes fragmented with the formation of MMA with either of the wavelengths, 5 eV photons do not supply enough thermal energy for ejection of large pieces of material. Therefore, the photon energy in addition to the number of photons is important in setting off photothermal ejection.

The Norrish type II simulations with a 5 ps pulse width do not see the shift in the ablation threshold using 5 eV photons due to the rapid formation of small molecules and high pressure that is present. Since most of the reactions occur within 1–2 ps following bond cleavage, more 5 eV photons are able to break the main chain bond rather than heat the material, e.g., at a fluence of 12 mJ/cm² with 5 eV/photon, 76% of the photons photochemically cleave the main chain bond using a 5 ps pulse width compared with 51% using a 150 ps pulse. The number of photons causing photolytic scissions is instrumental in the subsequent rapid formation of small particles and a pressure wave. For example, a maximum pressure of 4.8 GPa is observed at a fluence of 12 mJ/cm² with the 5 ps pulse compared with 1 GPa at the same fluence with the 150 ps pulse. The result is a more fragmented substrate with ejection driven by pressure using a 5 ps pulse. The Norrish type I simulations do not include the unzipping reactions, and hence the variance in yield is not observed with changing pulse width. The bond scissions occur on the side chain and do not result in monomer formation, which allows every photon to photochemically break a C–CO bond.

3. Plume Composition. The composition of the plume following ablation is consistent with the mechanisms described. Figure 5 displays the yield of small molecules (defined here as an MMA monomer or smaller) in units of MMA equivalents that have been ejected from the substrate as a function of fluence using 7.9 eV/photon and 5 eV/photon for (a) 5 ps and (b) 150

ps pulse widths. The Norrish type I results show a greater number of small molecules released at any given fluence using 5 eV photons which is indicative of the greater transformation deeper within the substrate due to the greater amount of photons. Even though the amount of total material ejected is greater using 5 eV photons, the composition of particles in the plume is approximately the same with a majority of the plume consisting of CO₂, CH₄, and large polymer clusters. The yield of small molecules for the Norrish type II simulation using 5 eV photons, however, is consistently less than the 7.9 eV/photon simulations for either the 5 ps or 150 ps pulse width. In comparison to the Norrish type I simulations, where the smaller molecules such as CO, CO₂, and CH₃OH that are produced are able to diffuse out of the material, Norrish type II simulations produce MMA monomers and polymer fragments which are less mobile. For the 7.9 eV/photon simulations, the ablation plume consists of many MMA monomers and MMA fragments in addition to several large polymer chunks. In contrast, the 5 eV ablation plumes mainly consist of one to three large pieces of substrate and very few monomer or monomer fragments. Simulations at both wavelengths produce MMA monomers, but the 7.9 eV photons dispense enough residual thermal energy after the photolytic scission to break up large pieces of material which consist of a mixture of polymers, polymer fragments, and monomers.

Several facets of this study are complementary to experimental findings. Experiments using nanosecond pulses have measured a mixture of gases, monomers, and polymer fragments in the ablation plume.^{19,21,22} From the simulations, the ablation plume is determined to consist of gases and clusters for Norrish type I decomposition of PMMA and monomers and large clusters for Norrish type II decomposition. While this result cannot directly correlate to experimental findings, it does indicate the complexity in each mechanism which occurs during photochemical ablation. Further experimental investigations of the species present in the plume and the distribution of their velocities, for example using 266 nm or lower wavelength radiation and short pulses, can shed light on the importance of each pathway in the ablation process.

Conclusions

In this article, the effects of chemical reactions, the formation of molecules, the amount of photons and energy deposition were studied for two photon energies interacting with a PMMA substrate. Two particular pathways of chemical breakdown following a photolytic scission were used—in one case, the

Norrish type I, small molecules and gases are formed, and in the other, Norrish type II, there is activated monomer unzipping. The lower energy photons ablate more material at equal fluences due to more photons causing fragmentation and chemical transformation deeper within the substrate. If the bond break event competes with heating, the fragmented substrate has to be sufficiently heated to thermally eject the material. This effect shifts the ablation threshold to a higher fluence for simulations using 5 eV photons with Norrish type II reactions and a pulse width of 150 ps. At equal fluences, the residual photon energy using 5 eV/photon heats the substrate less. The ablation plume composition does not change for the Norrish type I simulation with varying photon energy. However, for the Norrish type II simulations, the extra photon energy using the 7.9 eV photons allows the large pieces of material to thermally decompose which is reflected in the plume composition. Even though there are more photons available at a given fluence using lower energy photons than were used in this investigation, the ability for single photons to cleave bonds and to directly initiate photochemical reactions becomes energetically prohibitive. For those cases, the thermal effects and multiple photon absorption events then are extremely important in determining the amount of material transformation and the mechanism of ejection that occurs.

This study sheds insight into the mechanistic process of ejection using two different photon excitation energies. The contributions of the different Norrish type processes help in understanding the complexity of the relationship between the photon energy and the number of photons at a given fluence. Though the experimental absorption depth varies with wavelength and both reactions are likely to occur during the laser pulse, the simulations give a fundamental description of the ablation phenomenon and provide an account of the microscopic details that occur with differing amounts of photons and energies. Future studies will probe the mechanistic process of polymer ablation by varying the penetration depth, including multiple photon absorption events and using photons of longer wavelengths.

Acknowledgment. This work was supported by the National Science Foundation through the Information Technology and Research Program, Grant 0426604, and the U.S. Air Force Office of Scientific Research through the Multi-University Research Initiative. Computer support was provided by the Graduate Education and Research Services at Penn State University. The authors thank Yaroslava Yingling for her insight and helpful discussions.

References and Notes

- (1) Dyer, P. E. *Appl. Phys. A* **2003**, *77*, 167.
- (2) Roberts, M.; Rossier, J.; Bercier, P.; Girault, H. *Anal. Chem.* **1997**, *69*, 2035.
- (3) Bityurin, N. *Annu. Rep. Prog. Chem., Sect. C, Phys. Chem.* **2005**, *101*, 216.
- (4) Bityurin, N.; Luk'yanchuk, B. S.; Hong, M. H.; Chong, T. C. *Chem. Rev.* **2003**, *103*, 519.
- (5) Lippert, T.; Hauer, M.; Phipps, C. R.; Wokaun, A. *Appl. Phys. A* **2003**, *77*, 259.
- (6) Srinivasan, R. *Science* **1986**, *234*, 559.
- (7) Srinivasan, R. *Appl. Phys. A* **1993**, *56*, 417.
- (8) Srinivasan, V.; Smrtic, M. A.; Babu, S. V. *J. Appl. Phys.* **1986**, *59*, 3861.
- (9) Luk'yanchuk, B.; Bityurin, N.; Anisimov, S.; Bauerle, D. *Appl. Phys. A* **1993**, *57*, 367.
- (10) Kalontarov, L. I.; Marupov, R. *Chem. Phys. Lett.* **1992**, *196*, 15.
- (11) Garrison, B. J.; Srinivasan, R. *J. Appl. Phys.* **1985**, *57*, 2909.
- (12) Wu, X. W.; Sadeghi, M.; Vertes, A. *J. Phys. Chem. B* **1998**, *102*, 4770.
- (13) Yingling, Y. G.; Garrison, B. J. *Nucl. Instrum. Methods Phys. Res., Sect. B* **2003**, *202*, 188.
- (14) Zhigilei, L. V.; Kodali, P. B. S.; Garrison, B. J. *J. Phys. Chem. B* **1997**, *101*, 2028.
- (15) Zhigilei, L. V.; Leveugle, E.; Garrison, B. J.; Yingling, Y. G.; Zeifman, M. I. *Chem. Rev.* **2003**, *103*, 321.
- (16) Dyer, P. E.; Srinivasan, R. *Appl. Phys. Lett.* **1986**, *48*, 445.
- (17) Srinivasan, R.; Braren, B.; Seeger, D. E.; Dreyfus, R. W. *Macromolecules* **1986**, *19*, 916.
- (18) Srinivasan, R.; Braren, B. *Appl. Phys. Lett.* **1988**, *53*, 1233.
- (19) Küper, S.; Modaresi, S.; Stuke, M. *J. Phys. Chem.* **1990**, *94*, 7514.
- (20) Srinivasan, R.; Braren, B.; Casey, K. B. *J. Appl. Phys.* **1990**, *68*, 1842.
- (21) Krajnovich, D. J. *J. Phys. Chem. A* **1997**, *101*, 2033.
- (22) Blanchet, G. B.; Cotts, P.; Fincher, C. R. *J. Appl. Phys.* **2000**, *88*, 2975.
- (23) Costela, A.; Garciamoreno, I.; Florido, F.; Figuera, J. M.; Sastre, R.; Hooker, S. M.; Cashmore, J. S.; Webb, C. E. *J. Appl. Phys.* **1995**, *77*, 2343.
- (24) Fedynshyn, T. H.; Kunz, R. R.; Sinta, R. F.; Goodman, R. B.; Doran, S. P. *J. Vac. Sci. Technol. B* **2000**, *18*, 3332.
- (25) Estler, R. C.; Nogar, N. S. *Appl. Phys. Lett.* **1986**, *49*, 1175.
- (26) Tsunekawa, M.; Nishio, S.; Sato, H. *J. Appl. Phys.* **1994**, *76*, 5598.
- (27) Prasad, M.; Conforti, P. F.; Garrison, B. J. *J. Appl. Phys.* **2007**, *101*, 103113.
- (28) Prasad, M.; Conforti, P. F.; Garrison, B. J.; Yingling, Y. G. *Appl. Surf. Sci.* **2007**, *253*, 6382.
- (29) Yingling, Y. G.; Garrison, B. J. *Appl. Surf. Sci.* **2007**, *253*, 6377.
- (30) Yingling, Y. G.; Garrison, B. J. *J. Phys. Chem. B* **2005**, *109*, 16482.
- (31) Prasad, M.; Conforti, P. F.; Garrison, B. J. *J. Chem. Phys.*, in press.
- (32) Srinivasan, R.; Braren, B.; Casey, K. B. *Pure Appl. Chem.* **1990**, *62*, 1581.
- (33) Noyes, W. A., Jr. The Contributions of R. G. W. Norrish to Photochemistry. In *Photochemistry and Reaction Kinetics*; Ashmore, P. G., Dainton, F. S., Sugden, T. M., Eds.; Cambridge University Press: Cambridge, 1967; pp 1.
- (34) Preuss, S.; Späth, M.; Zhang, Y.; Stuke, M. *Appl. Phys. Lett.* **1993**, *62*, 3049.
- (35) Yingling, Y. G.; Garrison, B. J. *J. Phys. Chem. B* **2004**, *108*, 1815.
- (36) Lippert, T.; Webb, R. L.; Langford, S. C.; Dickinson, J. T. *J. Appl. Phys.* **1999**, *85*, 1838.
- (37) Conforti, P. F.; Garrison, B. J. *Chem. Phys. Lett.* **2005**, *406*, 294.
- (38) Good, D. A.; Francisco, D. S. *J. Phys. Chem. A* **2002**, *106*, 1733.
- (39) Kim, W. K.; Hayden, L. M. *J. Chem. Phys.* **1999**, *111*, 5212.
- (40) Zhigilei, L. V.; Garrison, B. J. *Mater. Res. Soc. Symp. Proc.* **1999**, *538*, 491.
- (41) Zhigilei, L. V.; Garrison, B. J. *J. Appl. Phys.* **2000**, *88*, 1281.
- (42) Hare, D. E.; Franken, J.; Dlott, D. D. *J. Appl. Phys.* **1995**, *77*, 5950.
- (43) Conforti, P. F.; Prasad, M.; Garrison, B. J. *Appl. Surf. Sci.* **2007**, *253*, 6386.